NJC

PAPER

View Article Online
View Journal | View Issue

Cite this: *New J. Chem.*, 2015, 39, 6274

Conformational insights and vibrational study of a promising anticancer agent: the role of the ligand in Pd(II)–amine complexes†

Sónia M. Fiuza,*[a] Ana M. Amado,[a] Stewart F. Parker,[b] Maria Paula M. Marques[ac] and Luís A. E. Batista de Carvalho[a]

Received (in Montpellier, France) 30th April 2015,
Accepted 2nd June 2015

DOI: 10.1039/c5nj01088h

www.rsc.org/njc

A conformational and vibrational analysis of an antiproliferative spermine-based dinuclear Pd(II) complex (Pd_2-Spm) is reported. Density functional theory coupled to all-electron basis sets was used to perform quantum mechanical calculations aimed at determining the strategy best suited for accurately representing this molecule and achieving an optimal accordance with the experimental data. The structural parameters and the vibrational frequencies predicted by the calculations are compared with the corresponding experimental data. The results support a relationship between the strength of the metal-ligand bonds and the antitumor activity of the compound.

1. Introduction

Palladium(II) complexes are an emerging class of inorganic compounds bearing recognizable anticancer properties,[1–5] challenging the initial belief that complexes containing this metal centre would be inactive. This conviction started to materialize with the lack of biological activity of the parent compound *cis*-diamminedichloropalladium(II) (cDDPd),[6] as opposed to its Pt(II) homologue (cisplatin, *cis*-diamminedichloroplatinum(II), cDDP) that was justified by the higher lability of palladium(II) complexes relative to platinum(II) ones. However, this problem has been circumvented by different synthetic strategies, most of them aimed at lowering this kinetic lability by coordination of the metal by polydentate or bulky ligands, yielding compounds with interesting therapeutic properties, largely determined by the nature of the ligands.[7–12] Kovala-Demertzi and co-workers[13] published an interesting study in which the substitution of a hydrogen for a methyl group in a bulky ligand has turned a biologically inactive compound into an active one. This shows that there is still much to be understood at the molecular level to unveil the physico–chemical phenomena that determine the behaviour of these metal-based compounds in living systems – their structure–activity relationships (SARs) being of paramount importance. Pd(II) complexes are particularly interesting compounds to perform SAR's studies, as the effect of the ligand on their biological activity is generally more pronounced than for their Pt(II) counterparts.

The present study focuses on a polynuclear Pd(II) chelate with a biogenic polyamine (spermine) – {μ-{*N*,*N*′-bis[(3-amino-κ*N*)-propyl]butane-1,4-diamine-κ*N*:κ*N*′}} tetrachloro-dipalladium (II), Pd_2-Spm (Fig. 1A).[14]

This complex was shown to display interesting antiproliferative properties against cancer cells,[15,16] although it presents a quite different chemical composition and structure from the array of active Pd(II) compounds reported in the literature to date. An understanding of the SARs determining this type of compound's activity is fundamental for interpreting the biochemical mechanisms underlying their biological effect (*e.g.* cytotoxicity), thus allowing a rational design of new Pd-based anticancer drugs. Vibrational spectroscopy has proven to be one of the most powerful techniques for performing conformational studies in biologically relevant molecules (including inorganic compounds). Inelastic neutron scattering (INS) spectroscopy is particularly well suited to study materials containing hydrogen atoms, since the scattering cross-section for hydrogen (^{1}H) (about 80 barns) is considerably larger than for most other elements (at most *ca.* 5 barns). The neutron scattering cross-section of an element is a characteristic of each isotope and independent of the chemical environment. During the scattering event, a fraction of the incoming neutron energy can be used to cause vibrational excitation, and the vibrational modes with the largest hydrogen displacements will dominate the spectrum. Therefore, INS can be especially important in solids in which the molecular units

[a] *Unidade de I&D "Química-Física Molecular", Departamento de Química, Universidade de Coimbra, P-3004 535 Coimbra, Portugal. E-mail: sonia.mfiuza@gmail.com; Fax: +351-239-826541; Tel: +351-239-826541*
[b] *ISIS Facility, SFTC Rutherford Appleton Laboratory, Chilton, Didcot, OX 11 0QX, UK*
[c] *Departamento de Ciências da Vida, P-3000 456, Universidade de Coimbra, Coimbra, Portugal*

† Electronic supplementary information (ESI) available. See DOI: 10.1039/c5nj01088h

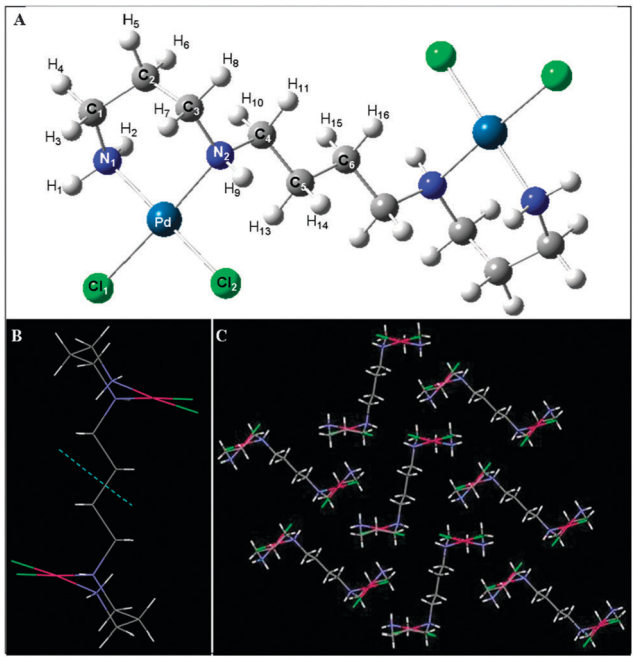

Fig. 1 (A) Optimized structure (LANL2DZ/6-31G*) for the Pd_2-Spm isolated molecule and the atom numbering scheme. (B) X-ray structure for Pd_2-Spm (preferred conformation in the solid state with the inversion center highlighted by the blue dashed line). (C) Crystal structure arrangement for Pd_2-Spm.

are linked together by close hydrogen contacts, with the lowest-frequency vibrations expected to be most affected. Combining experimental vibrational spectroscopy results with quantum mechanical calculated data allows a deeper understanding of the correlation between the system's molecular properties (structure and conformation) and the corresponding spectra.

In this study, quantum mechanical calculations were carried out for Pd_2-Spm at the DFT level, since this approach has been shown to deliver accurate results for this type of system.[17–19] A theoretical model previously reported by the authors for a mononuclear Pd(II) compound bearing non-chelating ligands[17] was presently evaluated because of its suitability for the highly flexible polynuclear polydentate chelate Pd_2-Spm. The accuracy of the calculated results was assessed by comparison with the experimental data available on this chelate – both studies reported X-ray structural information[14] and the vibrational results gathered in this work.

2. Experimental

2.1 Synthesis of Pd_2-Spm

Potassium tetrachloropalladate(II) (K_2PdCl_4, 98%) and spermine (≥97%) were acquired from Sigma (Sintra, Portugal) and used without further purification.

The synthesis of Pd_2-Spm was carried out following an optimized procedure based on the published synthetic route.[14] Briefly, 2 mmol of K_2PdCl_4 were dissolved in a minimal amount of water, and an aqueous solution containing 1 mmol of spermine was added dropwise under continuous stirring for about 24 h. Solid $(PdCl_2)_2$(Spm) was formed, which was filtered and washed with pure acetone. Upon drying in an oven at 40 °C overnight, yellow crystals were obtained.

Yield: 68%. Elemental analysis was carried out at the Atlantic Microlab, Inc., Georgia, USA. Calculated – C: 21.56%; H: 4.70%; N: 10.06%, Cl: 25.46% and Found: C: 21.22%; H: 4.68%; N: 9.60%, Cl: 25.88%.

2.2 Vibrational spectroscopy

Room-temperature Fourier transform Raman (FT-Raman) spectra were acquired using a Bruker RFS-100 Fourier transform Raman spectrometer, with near-infrared excitation provided by the 1064 nm line of a Nd:YAG laser. A laser power of 150 mW at the sample position was used. Each spectrum was the average of three repeated measurements of 150 scans at 2 cm^{-1} resolution.

Fourier transform infrared (FTIR) spectra at room temperature were recorded over the 400–4000 cm^{-1} region, with a Mattson 7000 FTIR spectrometer, using a globar source, a deuterated triglycine sulfate (DTGS) detector and potassium bromide pellets. Each spectrum was composed of 32 scans with 2 cm^{-1} resolution and triangular apodization.

The INS spectrum of the complex was obtained at the ISIS Pulsed Neutron Source of the STFC Rutherford Appleton Laboratory (United Kingdom), using the TOSCA spectrometer, an indirect geometry time-of-flight, high resolution (*ca.* 1.25% of the energy transfer), and broad range spectrometer.[20] A crystalline sample of the complex (2–3 g) was wrapped in a 4 × 4 cm aluminium foil sachet, which filled the beam, and placed in a thin walled aluminium can. To reduce the impact of the Debye–Waller factor on the observed spectral intensity, the sample was cooled to *ca.* 15 K. Data were recorded in the energy range from 24 to 4000 cm^{-1} and converted to the conventional scattering law, $S(Q,\nu)$ *vs.* energy transfer (in cm^{-1}) through standard programs.

2.3 Computational details

All calculations were performed using the Gaussian 03W (G03W) package.[21] Both isolated molecule and two-molecule geometry were fully optimized by the Berny algorithm using redundant internal coordinates. While the initial conformational study was carried out without symmetry constraints, once the best conformer was selected, subsequent calculations were subject to symmetry constraints (C_i symmetry group). In all cases, vibrational frequency calculations were performed, at the same level of theory, to verify that the geometries corresponded to a real minimum in the potential energy surface (no negative eigenvalues) and to simulate the vibrational spectra.

Two approaches were used to describe the palladium atom: either by relativistic pseudopotentials developed by Hay and Wadt,[22] in a double-zeta splitting scheme, as implemented in G03W (keyword *LANL2DZ*) or by an all-electron (AE) contracted Gaussian basis set developed by Friedlander.[23] The inclusion of a polarization function at the Pd atom, by augmenting the valence shell with an *f*-function (ζ_{Pd} = 1.472), was also tested in combination with LANL2DZ.[24] For the non-metal atoms, several AE basis sets were tested: 6-31G*, 6-31G**, 6-31+G(2d)

Table 1 Theoretical levels considered in this study, using the mPW1PW functional

System	Basis set		
	Pd(II)[a]	Non-heavy atoms[b]	
Two-molecule model	LANL2DZ	6-31G*	
Isolated molecule	AE	6-31G*	
	AE	6-31G**	
	AE	6-31+G(2df)	
	AE	6-31G** (H) 6-31G* (C) 6-31+G(2d) (N) 6-31+G(2df) (Cl)	mix1
	AE	6-31G** (H) 6-31+G(2d) (C,N) 6-31+G(2df) (Cl)	mix2

[a] AE stands for the all electron basis set of Friedlander[23] used at the Pd(II) ion. [b] Basis sets used generally or specifically on each atom as specified in mix1 and mix2.

and 6-31+G(2df) (as defined in G03W), either alone or simultaneously in distinct combinations schemes for different atoms (mix 1 and mix 2), as described in Table 1. Natural bond orbital (NBO) analysis was also performed. The basis sets were tested at the DFT level, using the mPW1PW method which comprises a modified version of the exchange term of Perdew–Wang and the Perdew–Wang 91 correlation functional,[25,26] which has been shown to be advantageous over other DFT functionals for both linear amine ligands and their Pt(II)/Pd(II) complexes.[17,18,27] The B97D DFT, which includes semi-empirical corrections for dispersion, was also tested.[28] In order to account for the basis set superposition error (BSSE) in the two-molecule model calculation, geometries were optimized within the scheme of Boys–Bernardi[29] (as implemented in G03W, by the keyword *COUNTERPOISE*). The SCRF (self-consistent reaction field) calculations were performed considering the aqueous solution ($\varepsilon = 78.39$) using default parameters for the UAHF (united atom topological model) radii model.[21]

3. Results and discussion

3.1 Conformational analysis

The reported X-ray structure for the Pd_2-Spm molecule[14] (Fig. 1) comprises both $Pd(dap)Cl_2$ units (dap = 1,3-diaminopropane, $H_2N(CH_2)_3NH_2$) in a relative *trans* arrangement. The chelate ring assumes a chair conformation, while the central putrescine-like moiety has an all-*trans* geometry. Careful inspection of this crystalline lattice structure (Fig. 1C) suggests the formation of intermolecular H-bonds between the $Pd(dap)Cl_2$ fractions of adjacent molecules, namely, Cl_1;$Cl_2\cdots H_1$,$H_2(N_1)$ and $Cl_2\cdots H_9(N_2)$, as well as a $Cl_1\cdots H_{10}(C_4)$ interaction. The more hydrophobic methylene groups should not be involved in this type of close contact.

Taking the determined X-ray geometry as the starting point, a rotational conformational analysis was performed for the Pd_2-Spm isolated molecule (Fig. S1 of the ESI†), considering a previous work on the cDDPd mononuclear complex.[17] We were interested in testing the relative stability of different *cis*/*trans* conformations (regarding the two metal centres relative to each other), all-*trans* and non-*trans* configurations of the amine linker and the presence or absence of co-planarity of the metal centre relative to the central amine linker. The minimum energy conformer obtained for Pd_2-Spm differs significantly from the reported X-ray structure. As the present work aims to understand the properties of a molecule in the solid state, this type of single molecule conformational study may not be adequate to accurately represent these large polynuclear systems, since the intermolecular interactions between neighbouring molecules in the crystal lattice (Fig. 1C) impact their structure to a much larger extent than for mononuclear complexes playing a non-negligible role on the maintenance of the overall chelate's conformation. The number of rotational conformers makes this type of study prohibitive for a system such as this one as it is too large and presents too many degrees of freedom.

In fact, taking the isomer present in the solid state, we screened it with the license-free program Avogadro[30] (using a molecular mechanics universal force field (UFF)), which predicted 242 conformers. Twenty of them, among the ones with lowest energy, were chosen to perform a more thorough study (Fig. S1, ESI†) as we were interested mainly in testing the relative stability of *cis*/*trans* conformations (regarding the two metal centres relative to each other), all-*trans* and non-*trans* configurations of the amine linker and co-planarity regarding the metal centre relative to the central amine linker.

Although plane-wave calculations have been carried out by the authors[31–34] to predict solid state arrangements, this type of approach is not easily accessible for this particular dinuclear chelate due to the large dimensions of the corresponding unit cell. In view of these limitations, and taking into account the aim of this study, to predict the properties of Pd_2-Spm in the solid state, the lowest-energy conformer found for the isolated molecule (conformer 1, Fig. S1, ESI†) was not considered in further analysis, but rather the optimized Pd_2-Spm isolated molecule that matches the X-ray data (Fig. 1A) was used.

3.2 Structural analysis

The single molecule of Pd_2-Spm taken from the X-ray file, which was previously optimized without symmetry constraints (conformer 5, Fig. S1, ESI† and Fig. 1A), was then re-optimized under symmetry constraints (C_i symmetry group), yielding the structural parameters shown in Table 2. The differences between the experimental and calculated values (Δ-values), and the corresponding overall errors ($\Delta\Delta$-values), calculated as previously described for cisplatin,[18] are also shown. In general, the larger deviations from the experimental values are verified for the $Pd(dap)Cl_2$ moiety. It was hypothesized that these could be mainly due to (i) poor description of the metal centre and/or (ii) neglecting the intermolecular interactions present in the crystal lattice.

Considering hypothesis (i), the LANL2DZ ECP was augmented with an *f*-polarization function at the Pd centre and the all-electron basis set of Friedlander[23] was tested on the metal ion. While augmenting the Pd valence shell did not lead to a significant

Table 2 Experimental and calculated (mPW1PW) structural parameters for Pd_2-Spm, at different theoretical levels

		Theory level													
Structural parameter	Exp[a]	LANL2DZ/ 6-31G*	Δ^b	AE/ 6-31G*	Δ^b	AE/ 6-31G**	Δ^b	AE/ 6-31G+(2d)	Δ^b	AE/ mix1	Δ^b	AE/ mix2	Δ^b	SCRF LANL2DZ/6-31G*	Δ^b
Bond length/pm															
$Pd–N_1$	202.2	208.4	6.2	205.3	3.1	205.3	3.1	205.0	2.8	204.7	2.5	206.1	3.9	206.4	4.2
$Pd–N_2$	204.1	209.8	5.7	205.7	1.6	205.2	1.1	205.5	1.4	205.1	1.0	205.5	1.4	208.1	4.0
$Pd–Cl_1$	231.6	231.7	0.1	232.8	1.2	227.9	−3.7	233.0	1.4	232.4	0.8	228.7	−2.9	235.7	4.1
$Pd–Cl_2$	231.4	232.2	0.8	233.8	2.4	229.2	−2.2	233.9	2.5	233.3	1.9	230.6	−0.8	235.4	4.0
$N_1–C_1$	148.5	147.8	−0.7	147.2	−1.3	147.1	−1.4	147.2	−1.3	147.3	−1.2	147	−1.5	147.7	−0.8
$N_2–C_3$	148.7	147.5	−1.2	147.1	−1.6	147.3	−1.4	147.0	−1.7	147.1	−1.6	146.9	−1.8	148.4	−0.3
$C_1–C_2$	150.6	152.4	1.8	152.5	1.9	152.4	1.8	152.5	1.9	152.5	1.9	152.3	1.7	151.8	1.2
$C_2–C_3$	151.8	152.7	0.9	152.8	1.0	152.6	0.8	152.8	1.0	152.8	1.0	152.6	0.8	152.2	0.4
$C_4–C_5$	152.1	152.1	0.0	152.3	0.2	152.1	0.0	152.3	0.2	152.3	0.2	152.0	−0.1	152.0	−0.1
$C_5–C_6$	153.3	152.6	−0.7	151.5	−1.8	152.4	−0.9	151.5	−1.8	151.5	−1.8	152.0	−1.3	152.7	−0.6
$N_2–C_4$	148.8	147.8	1.0	147.8	−1.0	147.4	−1.4	147.7	−1.1	147.8	−1.0	147.0	−1.8	148.2	−0.6
Angles/°															
$Cl_1–Pd–Cl_2$	93.9	96.3	2.4	99.2	5.3	97.0	3.1	99.5	5.6	99.1	5.2	97.7	3.8	93.5	−0.4
$N_1–Pd–N_2$	90.3	92.0	1.7	91.9	1.6	91.8	1.5	92.1	1.8	92	1.7	91.7	1.4	89.7	−0.6
$N_1–Pd–Cl_1$	88.5	85.5	−3.0	84.3	−4.2	85.5	−3.0	84.0	−4.5	84.3	−4.2	85.6	−2.9	87.8	−0.7
$N_2–Pd–Cl_2$	87.5	86.1	−1.4	84.5	−3.0	85.7	−1.8	84.2	−3.3	84.5	−3.0	85.0	−2.5	89.0	1.5
$Pd–N_1–C_1$	114.8	113.8	−1.0	108.5	−6.3	113.2	−1.6	108.5	−6.3	108.5	−6.3	113.1	−1.7	114.3	−0.5
$Pd–N_2–C_3$	113.9	111.8	−2.1	112.4	−1.5	111.9	−2.0	112.4	−1.5	112.4	−1.5	112.5	−1.4	111.6	−2.3
$Pd–N_2–C_4$	113.0	115.5	2.5	112.1	−0.9	115.3	2.3	112.1	−0.9	112.1	−0.9	114.1	1.1	114.1	1.1
$N_1–C_1–C_2$	110.5	112.5	2.0	112.3	1.8	112.2	1.7	112.3	1.8	112.2	1.7	112.7	2.2	112.3	1.8
$N_2–C_3–C_2$	114.3	114.5	0.2	114.4	0.1	114.1	−0.2	114.3	0.0	114.3	0.0	114.2	−0.1	114.7	0.4
$C_1–C_2–C_3$	115.7	115.9	0.2	116.4	0.7	115.8	0.1	116.4	0.7	116.4	0.7	116.0	0.3	114.9	−0.8
$C_3–N_2–C_4$	113.0	113.7	0.7	115.1	2.1	113.9	0.9	115.2	2.2	115.0	2.0	114.2	1.2	112.9	−0.1
$N_2–C_4–C_5$	112.3	112.3	0.0	109.6	−2.7	111.7	−0.6	109.6	−2.7	109.6	2.7	112.0	−0.3	112.4	0.1
$C_4–C_5–C_6$	111.3	111.2	0.1	113.0	1.7	111.5	0.2	113.1	1.8	113.0	1.7	111.3	0.0	111.2	−0.1
$\Delta\Delta$			1.5		2.0		1.5		2.1		1.9		1.5		1.3

[a] Average values for identical bonds in the molecule.[14] [b] Δ = calculated value − experimental value.[18]

change (results not shown), the use of an AE basis set at the Pd ion caused clear changes in the complex's structural parameters. From analysis of Table 2, it is evident that the use of an AE basis set on Pd(II) greatly improves the prediction of the Pd–N bond length, which had been previously overestimated by all theoretical approaches. However, this leads to a worsening of the Pd–Cl bond lengths (as well as of some bond angles involving chlorine) in the following order: for the Pd–Cl bond, LANL2DZ/6-31G* > AE/mix1 > AE/6-31G* ~ AE/mix2 > AE/6-31G+(2d) > AE/6-31G**; for the Cl–Pd–Cl angle, LANL2DZ/6-31G* > AE/6-31G** > AE/mix2 > AE/mix1 ~ AE/6-31G* > AE/6-31G+(2d); for the Cl–Pd–N angle, LANL2DZ/6-31G* > AE/6-31G** > AE/mix2 > AE/mix1 ~ 6-31G* > AE/6-31G+(2d). Interestingly, the addition of a polarization function to the hydrogen atom (AE/6-31G* → AE/6-31G**) leads to a better overall agreement relative to the experimental values of the Cl–Pd–Cl and N–Pd–Cl angles, which is probably be due to a better description of the neighbouring molecular groups bearing hydrogens. However, including higher polarization functions on the non-hydrogen atoms (AE/6-31+G(2d)) did not lead to an enhancement of the overall $\Delta\Delta$ values. Coupling the AE basis set tested for Pd(II) with a combination of different AE basis sets for the remaining atoms (mix1 or mix2) yielded better $\Delta\Delta$ values but did not solve the problem entirely. While mix1, which involves more extensive basis sets for the chlorine and nitrogen atoms (Table 1), led to a significant improvement of the Pd–Cl bond length, it did not produce more accurate values for the bond angles. In turn, while mix2, which extends the improvement of the basis set to the carbon, chlorine and nitrogen atoms (Table 1), yields better Δ values for the angles, it worsens some of the bond lengths.

Regarding hypothesis (ii), calculations for a two-molecule species (Fig. S2, ESI†) based on the X-ray structure reported for the complex were performed to verify if accounting for intermolecular interactions could improve the results. Considering this model led to an improvement of the calculated Pd–N bond length, at the cost of a worsening of the values for the Pd–Cl bond (Table S1, ESI†). However, although the bond angles involving the metal centre were greatly improved, the overall error was not much lower than that obtained for the isolated molecule. The reason for this probably lies on the fact that two Pd_2-Spm molecules are not enough to represent all the intermolecular interactions occurring in the solid lattice, where one Pd_2-Spm entity is surrounded by six neighbouring molecules (Fig. 1C). Accounting for a six-molecule model using the present theoretical approach is, however, not feasible. A calculation for the two-molecule structure was also performed with the new B97D DFT, which accounts for dispersion corrections allowing a better description of the intermolecular interactions, but without significant improvement in the results (not shown). Although the structural experimental parameters are given for the solid state, SCRF results were also used to assess intermolecular interactions, not between similar molecules, but with other molecules such as the ones occurring when simulating an aqueous solution. The results

gathered in Table 2 show that, interestingly, SCRF results are the ones that present the lowest bond lengths deviations obtained for the linking amine fragment N_1–C_1–C_2–C_3–N_2 and N_2–C_4. It also presents the lowest deviation values for the Cl_1–Pd–Cl_2, N_1–Pd–N_2 and Cl_1–Pd–N_1 angles, the ones more prone to establish intermolecular interactions. The reason for an improvement of these results when compared to the two-molecule structures, even when comparing different physical states, may be the limitation of considering only a two-molecule system instead of a larger one with at least two layers of molecules below and above. These results shed some light and hope on a very accurate prediction when plane-wave tools become available for the study of these compounds.

The theoretical estimate of the chelate's structural parameters is of the utmost importance for the prediction of reliable SARs for the complex. When comparing the experimental bond lengths for different compounds of the same type, it is interesting to verify that within Pd_2-Spm, the Pd–N bonds (203.2 pm average value, Table 2) are shorter relative to the parent mononuclear compound cDDPd (206.0 pm),[35] while the Pd–Cl ones are longer (231.5 pm *vs.* 227.5 pm).[35] Natural bond orbital (NBO) calculations through the calculated Wiberg bond indices – an indicator that reflects the strength of the bond – also predict this trend, which is interestingly correlated with the biological activity of the complexes involved (Fig. 2). In fact, regarding the human breast cell line MDA-MB-231, the IC_{50} obtained at 24 h are for cDDPd $\geq$ 100 μM, for Pd(dap)Cl_2 $>$ 100 μM and for Pd_2-Spm = 4.7 μM.

The mode of action of this type of metal-based compound is recognized to be through interaction, *via* covalent binding, with DNA.[36,37] Although the exact mechanism for Pd(II) complexes is not as well established as for their Pt(II) analogues, they are expected to have a rather similar behaviour due to their similar chemical characteristics. The anticancer properties of the well-known chemotherapeutic drug cisplatin relies on the binding of Pt(II) to the nitrogen (N^7) of the DNA bases.[36–38] This step must be preceded by an intracellular drug activation process through aquation, which involves the hydrolysis of the chlorine ligands. Accordingly, it is expected that the DNA binding ability of these amine-based Pd(II) complexes increases with weakening of the Pd–Cl bonds, as evidenced in Fig. 2. Although more systems are needed for an unequivocal and reliable correlation, these results prompt the investigation of this possible correlation and stress the importance of this type of study, even if in the solid state.

3.3 Vibrational analysis

Pd_2-Spm has 132 vibrational modes, 66 of A_u symmetry (infrared active) and 66 bearing A_g symmetry (Raman active). All the modes are INS active, since there are no selection rules for this non-optical vibrational spectroscopy technique (Fig. 3).

The assignment of the vibrational spectra of Pd_2-Spm, as well as the calculated wavenumber at the LANL2DZ/6-31G* theory level, are presented in Table 3. It has been shown previously that the small enhancement obtained with higher theory levels is not worth the associated computational cost.[17,18] Some vibrational modes (as well as the corresponding nomenclature used throughout the text) are schematically represented in Fig. 4.

As the metal units are linked by the aliphatic amine spermine, some low frequency vibrations are similar to the reported LAM and TAM modes previously assigned for this polyamine.[40,41] However, they were given alternative designations in this work since Pd-coordinated Spm does not constitute a free "linear bead system", as illustrated in Fig. 4.

The inspection of Fig. 3 allows us to determine the importance and complementarity of the different techniques used. Raman spectroscopy features more intense CH_2 stretching bands and also presents more prominent bands regarding the metal atom centres. In addition, the different bands from the organic parts of the molecule are not quite well resolved, appearing broad and overlapped. Nonetheless, the resolution of the band relative to the metal centre using the Raman technique allows us to distinguish the different vibrational frequencies, particularly for the Pd–N bond. As the environment of Pd–N_1 is different from Pd–N_2, these modes are not degenerate and it is possible to identify 4 bands for the νPd–N vibration instead of 2 bands if their environment was the same, *i.e.*, having a symmetrical centre.

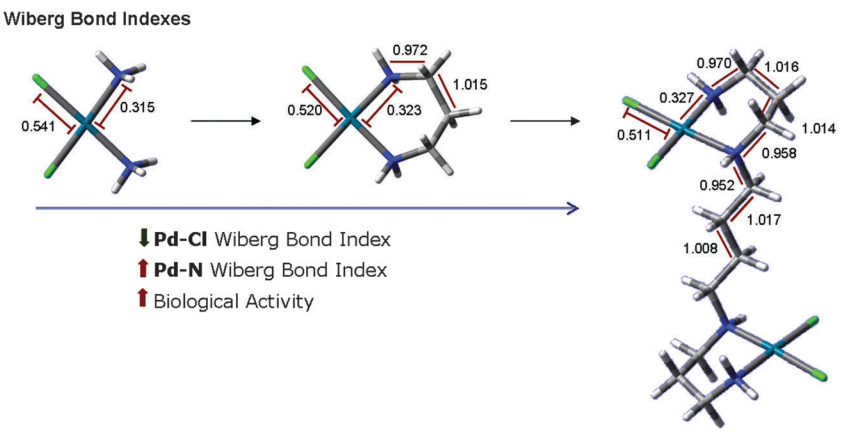

Fig. 2 Variation of Wiberg bond indices (WBI) for three different Pd(II) complexes: cDDPd (*cis*-diamminodichloropalladium(II)), Pd(dap)Cl_2 (1,3-diammino-propane-dichloropalladium(II)) and Pd_2-Spm ({μ-{*N*,*N*′-bis[(3-amino-κ*N*)propyl]butane-1,4-diamine-κ*N*:κ*N*′}} tetrachloro-dipalladium (II)). (White – H; Grey – C; Blue – N; Green – Cl; Cyan – Pd(II)). IC_{50} values for the MDA-MB-231 cell line at 24 h are $\geq$ 100 μM, $>$100 μM and 4.7 μM.

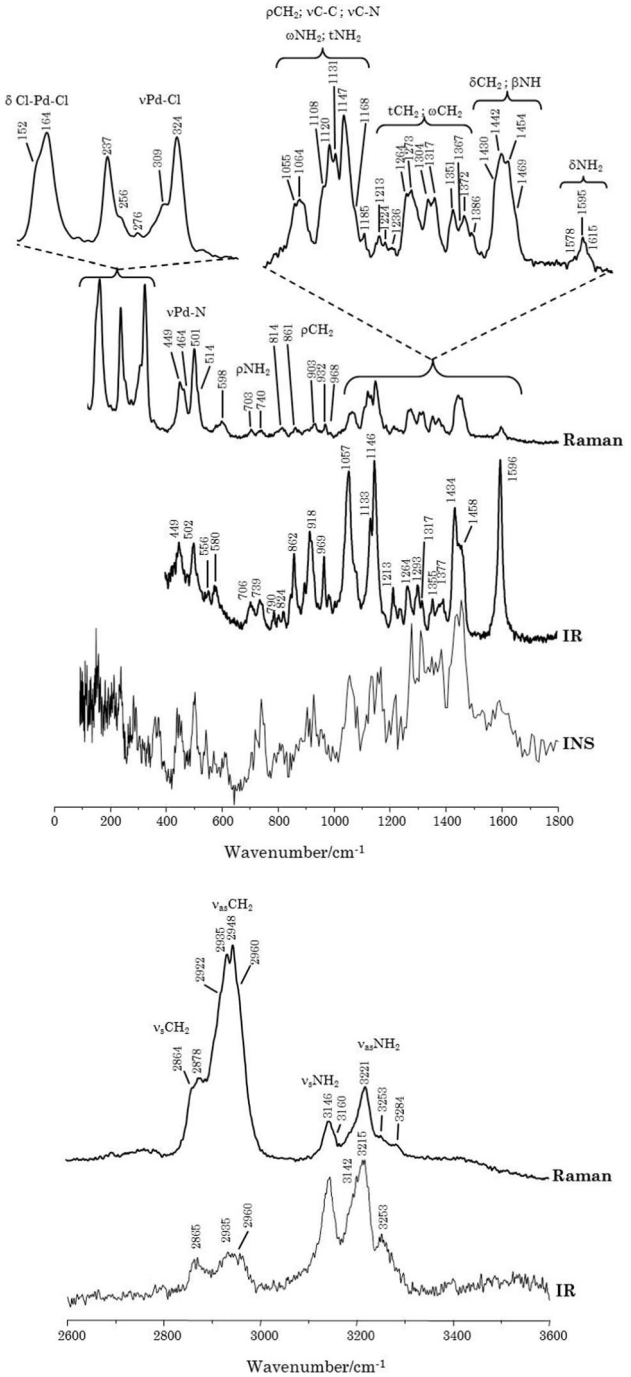

Fig. 3 Experimental vibrational spectra (Raman, IR and INS) for Pd_2-Spm.

This feature is not as clear when using the other vibrational techniques. IR and INS bands in turn appear much more defined in the region of 400–1800 cm^{-1} allowing the detection of a higher number of vibrational modes. Particularly important and characteristic of the IR technique is the very intense and well defined deformation band of NH_2 at 1596 cm^{-1}. When analysing the crystal structure packing unit, only one intermolecular hydrogen bond is available to the NH_2 group $(N_1)H_2$–Cl_2 (248.2 angstrom), and the next shortest contact for NH_2 is a weak intramolecular interaction $(N_1)H_1$–Cl_1 (268.7 angstrom). This well-defined δNH_2 band supports this occurrence as it is not as broad as the one expected for a group highly involved in strong hydrogen bonding. The INS technique in turn perfectly resolves the lower rocking modes of the CH_2 and NH_2 oscillators (almost imperceptible by Raman), as well as the ring structure torsion bands (almost absent from the IR and Raman spectra). These features stress the importance of using complementary vibrational techniques, especially for this type of complex, which tends to form intramolecular ring structures.

The vibrational modes of the spermine ligand were reasonably well predicted by the calculations, despite some deviations due to anharmonicity and/or intermolecular interactions. The major differences were verified for the modes involving the atoms directly bound to the metal atom, which cannot be justified in terms of anharmonicity since there is not a uniform pattern in the prediction of the wavenumbers. In order to determine whether this was a particular effect of this chelate, calculations were performed, at the same theory level (LANL2DZ/6-31G*), for a few other Pd(II) complexes with different amine ligands. The data thus gathered is shown in Table 4 as well as the scaling factor needed to match the calculated wavenumbers to the experimental ones. In every case, the theoretically predicted Pd–N stretching mode was found to be underestimated, while ν(Pd–Cl) and $\nu(NH_3/NH_2)$ were overestimated. Hence, this lack of accordance is independent of the type of complex investigated, and the main issue probably remaining is the description of the modes involving the metal centre.

In addition, neither the AE approach to describe the metal centre nor the two-molecule model calculations led to a noticeable improvement of the corresponding vibrational modes. In fact, it was previously verified by the authors[17] that an enhancement in the calculated structural parameters is not always accompanied by a corresponding improvement in the accuracy of the vibrational frequencies.

Although a straightforward comparison with the SCRF results (Table 3) cannot be performed, some interesting results can be observed. Actually, the vibrations relative to the stretching modes of NH_2 and CH_2 groups are greatly improved and comparable to the experimental values. Moreover, the symmetric stretching mode of Pd–N is also improved, but not the antisymmetric one. A better agreement with the experimental value is also obtained for the C–N–C torsion of the ring structure. However, many other vibrational modes are poorly predicted, such as the NH_2 and CH_2 scissoring and most wagging, twisting and rocking modes of the CH_2 groups. Moreover, many stretching vibrational modes for the C–C and C–N bonds fail to be predicted, as well as the ν(Pd–Cl) ones. Nonetheless, the improvement obtained for the groups expected to be strongly involved in intermolecular interactions should be of reference for future studies on this type of systems.

4. Conclusions

In the present work, a complete vibrational study of a dinuclear Pd(II) complex displaying a promising antiproliferative activity

Table 3 Experimental (INS, Raman, FTIR) and calculated (LANL2DZ/6-31G*) vibrational wavenumber (cm^{-1}) for Pd_2-Spm (isolated molecule in gas phase and simulated aqueous solution (SCRF))

Experimental								
INS	Raman	FTIR	Calc.	Calc. (scaled)[a]	Calc. SCRF	Calc. SCRF (scaled)[a]	Sym.	Tentative assignment[c]
		3253	3588	3408/3337[b]	3463	3290/3221[b]	A_u	$\nu_{as}NH_2$
	3221		3588	3408/3337[b]	3462	3289/3220[b]	A_g	$\nu_{as}NH_2$
		3215	3484	3309/3240[b]	3369	3200/3133[b]	A_u	νNH
			3484	3309/3240[b]	3367	3198/3131[b]	A_g	νNH
		3142	3483	3309/3239[b]	3363	3195/3128[b]	A_u	$\nu_s NH_2$
	3146		3483	3309/3239[b]	3362	3194/3127[b]	A_g	$\nu_s NH_2$
			3165	3006	3127	2970	A_u	$\nu_{as}CH_{2(ring)}$
			3165	3006	3126	2969	A_g	$\nu_{as}CH_{2(ring)}$
			3150	2992	3132	2975	A_u	$\nu_{as}CH_{2(chain)}$
		2960	3137	2980	3120	2964	A_u	$\nu_{as}CH_{2(ring)}$
	2960		3137	2980	3120	2964	A_g	$\nu_{as}CH_{2(ring)}$
2950	2948		3130	2973	3128	2971	A_g	$\nu_{as}CH_{2(chain)}$
	2935		3126	2969	3043	2891	A_g	$\nu_{as}CH_{2(ring)}$
		2935	3126	2969	3042	2890	A_u	$\nu_{as}CH_{2(ring)}$
			3112	2956	3110	2954	A_u	$\nu_{as}CH_{2(chain)}$
	2922		3110	2954	3094	2939	A_g	$\nu_{as}CH_{2(chain)}$
			3092	2937	3063	2910	A_u	$\nu_s CH_{2(chain)}$
			3087	2932	3069	2915	A_g	$\nu_s CH_{2(ring)}$
			3087	2932	3069	2915	A_u	$\nu_s CH_{2(ring)}$
			3085	2930	3056	2903	A_g	$\nu_s CH_{2(ring)}$
			3085	2930	3056	2903	A_u	$\nu_s CH_{2(ring)}$
	2878		3083	2929	3053	2900	A_g	$\nu_s CH_{2(chain)}$
			3078	2924	2999	2849	A_u	$\nu_s CH_{2(ring)}$
			3078	2924	2995	2845	A_u	$\nu_s CH_{2(ring)}$
	2864		3051	2898	3040	2888	A_g	$\nu_s CH_{2(chain)}$
		2865	3051	2898	3038	2886	A_u	$\nu_s CH_{2(chain)}$
1601	1595		1699	1614/1580[b]	1661	1578/1545[b]	A_g	δNH_2
		1596	1699	1614/1580[b]	1660	1577/1544[b]	A_u	δNH_2
			1539	1462	1532	1455	A_u	$\delta CH_{2(chain)}$
	1469		1537	1460	1526	1450	A_g	$\delta CH_{2(chain)}$
1457		1458	1529	1452	1511	1435	A_u	$\delta CH_{2(ring)}$
	1454		1527	1450	1510	1434	A_g	$\delta CH_{2(ring)}$
1440		1449	1524	1448	1507	1431	A_u	$\delta CH_{2(ring)}$
	1442		1523	1447	1506	1431	A_g	$\delta CH_{2(ring)}$
			1511	1435	1509	1433	A_u	$\delta CH_{2(ring)}$
			1508	1432	1488	1413	A_g	$\delta CH_{2(ring)}$
		1434	1508	1432	1488	1413	A_u	$\delta CH_{2(chain)}$
	1430		1504	1429	1497	1422	A_g	$\delta CH_{2(chain)}$
			1486	1412	1517	1441	A_g	βNH
			1485	1411	1516	1440	A_u	βNH
1385	1386		1460	1387	1444	1372	A_g	$\omega CH_{2(chain)}$
		1377	1455	1382	1434	1362	A_u	$\omega CH_{2(chain)}$
	1372		1436	1364	1452	1379	A_g	$\omega CH_{2(ring)}$
1365			1432	1360	1451	1378	A_u	$\omega CH_{2(ring)}$
	1367		1431	1359	1428	1356	A_g	$\omega CH_{2(ring)}$
1351		1355	1424	1353	1415	1344	A_u	$\omega CH_{2(ring)}$
	1351		1406	1336	1400	1330	A_g	$\omega CH_{2(ring)}$
1338			1398	1328	1399	1329	A_u	$\omega CH_{2(ring)}$
1314		1317	1377	1308	1350	1280	A_u	$\tau CH_{2(chain)}$
	1317		1372	1303	1361	1285	A_g	$\tau CH_{2(ring)}$
1299	1304		1371	1302	1375	1293	A_g	$\omega CH_{2(chain)}$
		1293	1368	1299	1353	1282	A_u	$\tau CH_{2(ring)}$
			1361	1293	1347	1264	A_g	$\tau CH_{2(chain)}$
1278	1273		1348	1280	1297	1216	A_g	$\tau CH_{2(chain)}$
1256		1264	1334	1267	1331	1255	A_u	$\tau CH_{2(ring)}$
1240		1238	1304	1239	1280	1187	A_u	$\omega CH_{2(chain)}$
1218	1224		1295	1230	1321	1253	A_g	$\tau CH_{2(ring)}$
	1213		1287	1223	1319	1248	A_g	$\tau CH_{2(ring)}$
		1213	1281	1217	1314	1232	A_u	$\tau CH_{2(ring)}$
1163		1179	1261	1198	1250	1167	A_u	$\tau NH_2 + \tau CH_{2(chain)}$
	1185		1244	1182	1229	1143	A_g	$\tau NH_2 + \rho CH_{2(chain)}$
		1146	1184	1125	1170	1104	A_u	$\tau CH_{2(chain)} + \tau CH_{2(ring)}$
	1147		1167	1109	1112	1051	A_g	$\nu C–C$
1136	1131		1166	1108	1200	1120	A_g	$\rho CH_{2(chain)}$
		1133	1163	1105	1203	1140	A_u	ωNH_2
	1120		1142	1085	1112	1051	A_g	$\nu C–C$
			1130	1073	1162	1099	A_u	$\nu C–N$
	1108		1127	1071	1179	1111	A_g	ωNH_2

Table 3 (*continued*)

Experimental								
INS	Raman	FTIR	Calc.	Calc. (scaled)[a]	Calc. SCRF	Calc. SCRF (scaled)[a]	Sym.	Tentative assignment[c]
1085		1085	1122	1066	1157	1056	A_u	νC–N
			1107	1052	1101	1040	A_u	νC–N
1070	1064		1100	1045	1095	1031	A_g	νC–C$_{(chain)}$
1057	1055		1098	1043	1085	1031	A_g	νC–N
		1057	1092	1037	1016	951	A_u	νC–N
			1082	1028	1106	1046	A_g	γNH
			1065	1012	1085	1020	A_u	γNH
			1058	1005	1074	1018	A_g	νC–C
			1052	999	1001	920	A_g	νC–N
		969	1025	974	1072	965	A_u	νC–C
		918	977	928	968	912	A_u	νC–C
930	932		970	921	960	901	A_g	ρCH$_{2(ring)}$
		899	945	898	949	887	A_u	ρCH$_{2(chain)}$
906			939	892	934	885	A_u	ρCH$_{2(ring)}$
	903		937	890	932	857	A_g	ρCH$_{2(ring)}$
	861		884	840	902	854	A_g	ρCH$_{2(ring)}$
		862	883	839	899	796	A_u	ρCH$_{2(ring)}$
812	814		826	785	838	793	A_g	ρCH$_{2(ring)}$
789		790	823	782	835	773	A_u	ρCH$_{2(ring)}$
			811	770	814	714	A_g	ρCH$_{2(chain)}$
			750	712	752	712	A_u	ρCH$_{2(chain)}$
707/725/745		706/739	680	680	750	711	A_u	ρNH$_2$
	703/740		680	680	748	560	A_g	ρNH$_2$
612	598		572	572	590	558	A_g	β ring
576		579	560	560	587	500	A_u	β ring
544		552	549	549	502	477	A_u	δN–C–C$_{(ring)}$
	514		531	531	526	499	A_g	δC–N–C
			474	474	499	493	A_u	δC–N–C
504	501	502	437	485[b]	480	533[b]	A_u	ν_sPd–N
			436	484[b]	456	506[b]	A_g	ν_sPd–N
457	464		471	471	428	428	A_g	τCC$_{ring}$
450	449		398	442[b]	499	554[b]	A_g	ν_{as}Pd–N
442		449	393	436[b]	493	547[b]	A_u	ν_{as}Pd–N
	324	—	345	321[b]	320	298[b]	A_g	ν_sPd–Cl
		—	343	319[b]	319	297[b]	A_u	ν_sPd–Cl
361/375		—	337	337	280	280	A_u	γ ring
	309	—	326	303[b]	300	279[b]	A_g	ν_{as}Pd–Cl
295		—	315	293[b]	293	272[b]	A_u	ν_{as}Pd–Cl
286	276	—	282	262[b]	242	225[b]	A_g	δN–Pd–N
		—	281	261[b]	230	214[b]	A_u	δN–Pd–N
242	256	—	265	265	192	192	A_g	γ ring
236	237	—	249	249	310	310	A_g	βC–C–C "swinging"
216		—	222	222	349	349	A_u	"ring breathing"
		—	198	198	214	214	A_u	γ_1C–C–C$_{chain}$
196	203	—	185	205[b]	140	155[b]	A_g	δN–Pd–Cl
		—	179	199[b]	136	151[b]	A_u	δN–Pd–Cl
168	164	—	167	167	223	223	A_g	τC–N$_{ring}$
153	152	—	150	150	158	158	A_g	γ_2C–C–C$_{chain}$
160		—	148	148	117	117	A_u	γ_3C–C–C$_{chain}$
		—	142	142	143	143	A_u	δCl–Pd–Cl
		—	140	140	142	142	A_g	δCl–Pd–Cl
		—	127	127	110	110	A_g	γ_4C–C–C$_{chain}$
117		—	121	121	167	167	A_u	τC–N$_{ring}$
103		—	104	104	155	155	A_g	γ_5C–C–C$_{chain}$
		—	89	89	80	80	A_u	γN–Pd–Cl
		—	88	88	42	42	A_g	γN–Pd–Cl
		—	75	75	73	73	A_u	γ'N–Pd–Cl
		—	74	74	71	71	A_g	γ'N–Pd–Cl
		—	70	70	111	111	A_u	Skeletal modes
		—	52	52	98	98	A_g	Skeletal modes
30		—	32	32	31	31	A_u	Skeletal modes
25		—	26	26	26	26	A_g	Skeletal modes
		—	23	23	23	23	A_u	Skeletal modes
		—	11	11	6	6	A_u	Skeletal modes

[a] Wavenumbers above 700 cm^{-1} were scaled by 0.9499, accordingly to Merrick *et al.*[39] [b] Wavenumbers scaled by 3 different scaling factors $\lambda_1 = 0.93$, $\lambda_2 = 1.01$ and $\lambda_3 = 1.11$ where λ_1—νNH$_3$, δ_{as}NH$_3$, νPd–Cl, δN–Pd–N; λ_2—δ_sNH$_3$, ρNH$_3$, γN–Pd–Cl; λ_3—νPd–N, δN–Pd–Cl, according to Fiuza *et al.*[17] [c] ν = stretching; δ, β = in-plane deformation; ρ = rocking; τ = torsion; γ and γ' = in phase and out of phase out-of-plane deformation.

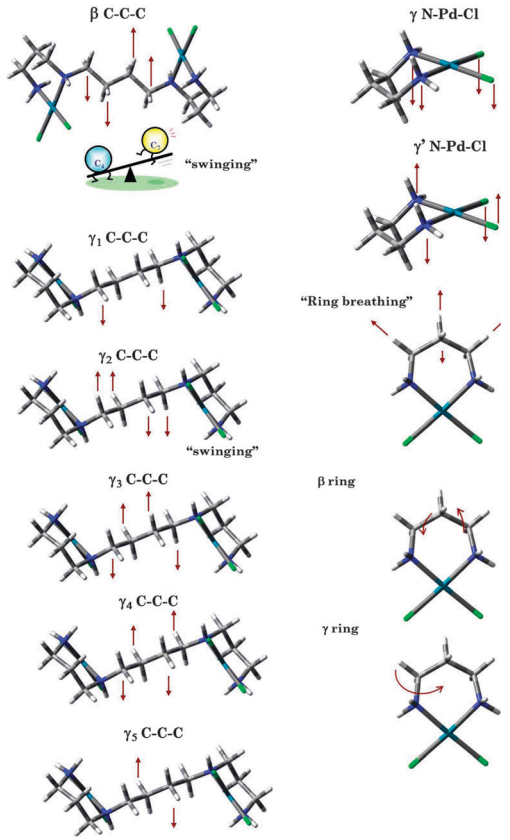

Fig. 4 Schematic of selected vibrational modes for Pd_2-Spm (and nomenclature used in this work).

Table 4 Calculated (mPW1PW/LANL2DZ/6-31G*) scaling factors for selected vibrational modes, regarding different Pd(II)–amine complexes

	Scaling factor for each vibrational mode		
Compound	$\nu NH_3/\nu NH_2$	νPd–N	νPd–Cl
cDDPd	0.91	1.13	0.93
$[Pd(NH_3)_4]\cdot 2Cl\cdot H_2O$	0.93	1.10	—
$[Pd(NH_3)_3(DMSO)]\cdot 2Cl$	0.92	1.11	—
$[PdCl_2(en)]$	0.91	1.07	0.90
$[PdCl_2(dap)]$	0.92	1.20	0.89
[Pd_2-Spm]	0.92	1.17	0.94
Average	0.92	1.13	0.92

was undertaken by a combined spectroscopic and quantum mechanical calculation methodology. FTIR, Raman and INS spectra were recorded and the theoretical analysis was carried out at the DFT level, for both the isolated molecule and a two-molecule model.

It was shown that the intermolecular interactions within the crystal lattice are of the utmost importance for this type of polynuclear polyamine chelate. A simple isolated molecule calculation was found not to suffice for predicting the molecular properties of such a system, in contrast to that reported (by the authors) for mononuclear counterparts. Although the calculations performed for the two-molecule species yielded slightly better results, the structural improvements were not noteworthy. Furthermore, when no X-ray data are available and several possible two-molecule geometries are to be tested, this approach becomes excessively demanding (in terms of computational costs).

In order to further improve the representation of this type of Pd(II)–amine complex, it is of paramount importance to develop new basis sets as recently undertaken for Pt(II) complexes[19,42] (which was beyond the scope of this work). At the moment, it seems that the precise estimate of one type of metal–ligand bond length leads to uncertainty in the other one, and an improvement of the bond lengths results in a worse description of the bond angles. Therefore, when considering only the prediction of the structural parameters, some doubts can arise as to the most suitable theoretical approach. For the representation of the vibrational profiles, in turn, the LANL2DZ/6-31G* theory level was shown to attain a high degree of agreement with the experiment, while the enhancement obtained with higher theory levels was not worth the associated computational cost. Optimization of the theoretical methodology for this type of Pd(II) polynuclear polyamine agent will hopefully allow the establishment of accurate and reliable SARs and enable the prediction of other important properties relevant to their anticancer activity. Finally, while plane-wave calculations are of utmost importance for estimating the properties of a molecule in the solid state, an up-to-date all-electron basis set for palladium(II) is also crucial, since studies for an isolated molecule cannot be ruled out for large polynuclear complexes bearing biological properties.

The data obtained in this work shows an inverse relationship between the strength of the Pd–Cl bond and the antiproliferative effect of Pd_2-Spm against cancer cells, *i.e.*, the weaker the Pd–Cl bonds the higher the complex's activity. The antiproliferative activity of such a compound is determined by several other factors. However, this evidence may indicate that these Pd(II)–amine chelates (comprising cisplatin-like moieties) could display a similar mode of action to that of cisplatin, involving chloride hydrolysis inside the cell as their major activation step.

Acknowledgements

The authors acknowledge financial support from the Portuguese Foundation for Science and Technology – UID/MULTI/00070/2013. SF thanks FCT – the Portuguese Foundation for Science and Technology – SFRH/BPD/75334/2010 scholarship. The INS work was supported by the European Commission under the 7th Framework Programme through the Key Action: Strengthening the European Research Area, Research Infrastructures (Contract no.: CP-CSA_INFRA-2008-1.1.1 Number 226507-NMI3). Laboratório Associado CICECO (University of Aveiro, Portugal) is also acknowledged for access to the FT-Raman and FTIR spectrometers.

References

1 S. Ray, R. Mohan, J. K. Singh, M. K. Samantaray, M. M. Shaikh, D. Panda and P. Ghosh, *J. Am. Chem. Soc.*, 2007, **129**, 15042–15053.
2 E. Gao, C. Liu, M. Zhu, H. Lin, Q. Wu and L. Liu, *Anti-Cancer Agents Med. Chem.*, 2009, **9**, 356–368.

3 F. Aria, B. Cevatemrea, E. I. I. Armutakb, N. Aztopala, V. T. Yilmazc and E. Ulukaya, *Bioorg. Med. Chem.*, 2014, **22**, 4948–4954.
4 A. Garoufis, S. K. Hadjikakou and N. Hadjiliadis, *Coord. Chem. Rev.*, 2009, **253**, 1384–1397.
5 E. Sindhuja, R. Ramesh, N. Dharmaraj and Y. Liu, *Inorg. Chim. Acta*, 2014, **416**, 1–12.
6 J. L. Butour, S. Wimmer, F. Wimmer and P. Castan, *Chem.-Biol. Interact.*, 1997, **104**, 165–178.
7 F. Shaheen, A. Badshah, M. Gielen, C. Gieck, M. Jamil and D. Vos, *J. Organomet. Chem.*, 2008, **693**, 1117–1126.
8 F. Shaheen, A. Badshah, M. Gielen, G. Croce, U. Florke, D. de Vos and S. Ali, *J. Organomet. Chem.*, 2010, **695**, 315–322.
9 H. A. El-Asmy, I. S. Butler, Z. S. Mouhri, B. J. Jean-Claude, M. S. Emmam and S. I. Mostafa, *J. Mol. Struct.*, 2014, **1059**, 193–201.
10 P. Vranec and I. Potocnak, *J. Mol. Struct.*, 2013, **1041**, 219–226.
11 R. A. Haque, A. W. Salman, S. Budagumpi, A. A. A. Abdullah and A. M. S. A. Majid, *Metallomics*, 2013, **5**, 760–769.
12 M. P. M. Marques, *ISRN Spectrosc.*, 2013, **2013**, 1–29.
13 D. Kovala-Demertzi, A. Alexandratos, A. Papageorgiou, P. N. Yadav, P. Dalezis and M. A. Demertzis, *Polyhedron*, 2008, **27**, 2731–2738.
14 G. Codina, A. Caubet, C. López, V. Moreno and E. Molins, *Helv. Chim. Acta*, 1999, **82**, 1025.
15 A. S. Soares, S. M. Fiuza, M. J. Gonçalves, L. A. E. Batista de Carvalho, M. P. M. Marques and A. M. Urbano, *Lett. Drug Des. Discovery*, 2007, **4**, 460–463.
16 S. M. Fiuza, J. Holy, L. A. E. Batista de Carvalho and M. P. M. Marques, *Chem. Biol. Drug Des.*, 2011, **77**, 477–488.
17 S. M. Fiuza, A. M. Amado, H. F. Dos Santos, M. P. M. Marques and L. A. E. Batista de Carvalho, *Phys. Chem. Chem. Phys.*, 2010, **12**, 14309–14321.
18 A. M. Amado, S. M. Fiuza, M. P. M. Marques and L. A. E. Batista de Carvalho, *J. Chem. Phys.*, 2007, **127**, 185104.
19 D. Paschoal, B. L. Marcial, J. F. Lopes, W. B. De Almeida and H. F. Dos Santos, *J. Comput. Chem.*, 2012, **33**, 2292–2302.
20 http://www.isis.stfc.ac.uk/.
21 M. J. Frisch, G. W. Trucks, H. B. Schlegel, G. E. Scuseria, M. A. Robb, J. R. Cheeseman, J. A. Montgomery Jr., T. Vreven, K. N. Kudin, J. C. Burant, J. M. Millam, S. S. Iyengar, J. Tomasi, V. Barone, B. Mennucci, M. Cossi, G. Scalmani, N. Rega, G. A. Petersson, H. Nakatsuji, M. Hada, M. Ehara, K. Toyota, R. Fukuda, J. Hasegawa, M. Ishida, T. Nakajima, Y. Honda, O. Kitao, H. Nakai, M. Klene, X. Li, J. E. Knox, H. P. Hratchian, J. B. Cross, V. Bakken, C. Adamo, J. Jaramillo, R. Gomperts, R. E. Stratmann, O. Yazyev, A. J. Austin, R. Cammi, C. Pomelli, J. W. Ochterski, P. Y. Ayala, K. Morokuma, G. A. Voth, P. Salvador, J. J. Dannenberg, V. G. Zakrzewski, S. Dapprich, A. D. Daniels, M. C. Strain, O. Farkas, D. K. Malick, A. D. Rabuck, K. Raghavachari, J. B. Foresman, J. V. Ortiz, Q. Cui, A. G. Baboul, S. Clifford, J. Cioslowski, B. B. Stefanov, G. Liu, A. Liashenko, P. Piskorz, I. Komaromi, R. L. Martin, D. J. Fox, T. Keith, M. A. Al-Laham, C. Y. Peng, A. Nanayakkara M. Challacombe, P. M. W. Gill, B. Johnson, W. Chen, M. W. Wong, C. Gonzalez and J. A. Pople, *Gaussian 03, Revision D.01*, Gaussian, Inc., Wallingford, CT, 2004.
22 P. J. Hay and W. R. Wadt, *J. Chem. Phys.*, 1985, **82**, 299–310.
23 M. E. Friedlander, J. M. Howell and G. Snyder, *J. Chem. Phys.*, 1982, **77**, 1921–1929.
24 A. W. Ehlers, M. Bohme, S. Dapprich, A. Gobbi, A. Hollwarth, V. Jonas, K. F. Kohler, R. Stegmann, A. Veldkamp and G. Frenking, *Chem. Phys. Lett.*, 1993, **208**, 111–114.
25 C. Adamo and V. Barone, *J. Chem. Phys.*, 1998, **108**, 664–675.
26 J. P. Perdew, K. Burke and Y. Wang, *Phys. Rev. B: Condens. Matter Mater. Phys.*, 1996, **54**, 16533.
27 S. Padrão, S. M. Fiuza, A. M. Amado, A. M. A. da Costa and L. A. E. Batista de Carvalho, *J. Phys. Org. Chem.*, 2011, **24**, 110–121.
28 S. Grimme, *J. Comput. Chem.*, 2006, **27**, 1787–1799.
29 S. F. Boys and F. Bernardi, *Mol. Phys.*, 1970, **19**, 558–566.
30 M. D. Hanwell, D. E Curtis, D. C. Lonie, T. Vandermeersch, E. Zurek and G. R. Hutchison, *J. Cheminf.*, 2012, **4**, 17.
31 R. L. Lopes, M. P. M. Marques, R. Valero, J. Tomkinson and L. A. E. Batista de Carvalho, *Spectrosc. Int. J.*, 2012, **27**, 273–292.
32 M. P. M. Marques, R. Valero, S. F. Parker, J. Tomkinson and L. A. E. Batista de Carvalho, *J. Phys. Chem. B*, 2013, **117**, 6421–6429.
33 R. L. Lopes, R. Valero, J. Tomkinson, M. P. M. Marques and L. A. E. Batista de Carvalho, *New J. Chem.*, 2013, **37**, 2691–2699.
34 M. P. M. Marques, L. A. E. Batista de Carvalho, R. Valero, N. F. L. Machado and S. F. Parker, *Phys. Chem. Chem. Phys.*, 2014, **16**, 7491–7500.
35 S. D. Kirik, L. A. Solovyov and M. L. Blokhina, *Acta Crystallogr., Sect. B: Struct. Sci.*, 1996, **52**, 909–916.
36 P. Banerjee, *Coord. Chem. Rev.*, 1999, **190–192**, 19–28.
37 A. Eastman, *Biochemistry*, 1983, **22**, 3927–3933.
38 M. Kartalou and J. M. Essigmann, *Mutat. Res.*, 2001, **478**, 1–21.
39 J. P. Merrick, D. Moran and L. Radom, *J. Phys. Chem. A*, 2007, **111**, 11683–11700.
40 M. P. M. Marques, L. A. E. Batista de Carvalho and J. Tomkinson, *J. Phys. Chem. A*, 2002, **106**, 2473–2482.
41 L. A. E. Batista de Carvalho, M. P. M. Marques and J. Tomkinson, *J. Phys. Chem. A*, 2006, **110**, 12947–12954.
42 R. C. De Berrêdo and F. E. Jorge, *THEOCHEM*, 2010, **961**, 107–112.